

Protective Nanosheet Coatings for Thiophosphate-Based All-Solid-State Batteries

Leonhard Karger, Barbara Nascimento Nunes, Yuriy Yusim, Andrey Mazilkin, Ruizhuo Zhang, Wengao Zhao, Anja Henss, Aleksandr Kondrakov, Jürgen Janek,* and Torsten Brezesinski*

Superionic sulfide solid electrolytes (SEs) are of considerable interest for application in solid-state batteries, but suffer from limited stability. When in combination with state-of-the-art cathode active materials (CAMs), severe degradation at the CAM/SE interface occurs during electrochemical cycling. To improve upon the interfacial stability, inert coatings can be applied to the CAM particles, with the goal of preventing direct contact to the SE. In this study, different methods of depositing coatings, including hexagonal boron nitride, tungsten sulfide and exfoliated $((\text{CH}_3(\text{CH}_2)_3)_4\text{N})_4\text{Nb}_6\text{O}_{17}$, in the form of nanosheets onto the free surface of a Ni-rich $\text{LiNi}_x\text{Co}_y\text{Mn}_z\text{O}_2$ (NCM) CAM are examined and compared with one another. While dry coating is shown to produce relatively uniform coatings (good surface coverage), the secondary particle morphology of the NCM makes ball milling as a mechanical deposition method less attractive. In contrast, deposition from dispersions in organic solvents yields protective coatings with a lower degree of surface coverage. The different materials are electrochemically tested in liquid- and solid-electrolyte-based lithium-ion batteries. A stabilizing effect from nanosheet coating is only observed for the cells with lithium thiophosphate SE.

batteries (SSBs) competitive with the established lithium-ion battery (LIB) technology.^[1–3] Among the existing superionic conductors, lithium thiophosphates stand out due to high ionic conductivity at room temperature and favorable mechanical properties for electrode/separator manufacturing and battery operation.^[4] When used as a catholyte, their reactivity toward energy-dense cathode active materials (CAMs), such as layered $\text{LiNi}_x\text{Co}_y\text{Mn}_z\text{O}_2$ (NCM or NMC) or $\text{LiNi}_x\text{Co}_y\text{Al}_z\text{O}_2$ (NCA), necessitates protective barriers to prevent degradation upon electrochemical cycling.^[5–7] Coating of the CAM particles is a promising strategy to achieve stable cathode interfaces (i.e., between NCMs and lithium thiophosphates).^[6,8]

Commonly employed coatings for SSB application are (lithiated) metal oxides of niobium or zirconium, which can be applied by different techniques, such as sol-gel chemistry,^[9–14] dry coating,^[15]

nanoparticle deposition^[16–18] or atomic layer deposition (ALD).^[19,20] Nanosheet coatings consisting of single or few atomic layers combine various beneficial properties, including high mechanical strength,^[21] chemical stability^[22] and gas

1. Introduction

Engineering of stable interfaces at both anode and cathode is one of the main challenges in making bulk-type solid-state

L. Karger, B. N. Nunes, A. Mazilkin, R. Zhang, W. Zhao, A. Kondrakov, J. Janek, T. Brezesinski
Battery and Electrochemistry Laboratory (BELLA)
Institute of Nanotechnology
Karlsruhe Institute of Technology (KIT)
Herrmann-von-Helmholtz-Platz 1, 76344 Eggenstein-Leopoldshafen,
Germany
E-mail: juergen.janek@phys.Chemie.uni-giessen.de;
torsten.brezesinski@kit.edu

Y. Yusim, A. Henss, J. Janek
Institute of Physical Chemistry & Center for Materials Research
(ZfM/LaMa)
Justus-Liebig-University Giessen
Heinrich-Buff-Ring 17, 35392 Giessen, Germany
A. Mazilkin
Karlsruhe Nano Micro Facility (KNMFi)
Karlsruhe Institute of Technology (KIT)
Herrmann-von-Helmholtz-Platz 1, 76344 Eggenstein-Leopoldshafen,
Germany
A. Kondrakov
BASF SE
Carl-Bosch-Str. 38, 67056 Ludwigshafen, Germany

 The ORCID identification number(s) for the author(s) of this article can be found under <https://doi.org/10.1002/admi.202301067>

© 2024 The Authors. Advanced Materials Interfaces published by Wiley-VCH GmbH. This is an open access article under the terms of the [Creative Commons Attribution](https://creativecommons.org/licenses/by/4.0/) License, which permits use, distribution and reproduction in any medium, provided the original work is properly cited.

DOI: 10.1002/admi.202301067

blocking ability.^[23] Furthermore, nanosheets are extremely thin (down to the theoretical limit of a single layer),^[24,25] thus barely affecting the battery's energy density (by introducing additional mass in the form of inactive material).

In recent years, some nanosheet materials have already been tested as CAM coatings in LIBs.^[26–30] Graphene takes a prominent position owing to its high stability and thoroughly researched properties and processing (including synthesis). Reduced graphene oxide is typically used to produce such carbon coatings due to facile deposition upon reduction, although some authors argue that surface modification or gaseous reducing agents are required, making the techniques experimentally challenging.^[31–34] Alternative methods relying on surfactant-stabilized graphene dispersions and allowing for controlled deposition have been reported.^[35] Hersam and coworkers elaborate on this approach by employing Pickering emulsions for preparing conformal graphene shells, ultimately aiming at high volumetric density cathodes by avoiding low-density carbon black, and decreasing porosity.^[26] Graphene coating is found, among others, to attenuate oxygen release from the cathode with cycling to high cutoff potentials (note: in the SSB case, oxygen loss would contribute to the decomposition of the thiophosphate solid electrolyte).^[27,36,37]

Apart from graphene, other nanosheet coatings and preparation methods have been reported. For example, layered double hydroxides were deposited from aqueous dispersions onto NCM and NCA both before and after calcination.^[28,38] Graphitic carbon nitride can also be deposited from aqueous dispersions or by chemical vapor deposition (CVD).^[39] Transition-metal chalcogenides, such as MoS₂ and WSe₂, have been shown to increase the stability of CAMs.^[29] Recently, Maiti et al. utilized CVD-grown WSe₂ for improving the cycling performance of NCM851005 (85% Ni content) and high-voltage LiNi_{0.5}Mn_{1.5}O₄ (LNMO). Stabilization is ascribed to reduced transition-metal leaching from the CAM particles, while the coating apparently dissolves to some degree into the electrode, which in turn helps to form a protective layer on the anode.^[29] Overall, nanosheet coatings have been employed successfully in LIBs and shown to facilitate charge transport^[26] and/or mitigate cathode and electrolyte degradation.^[29,31] Consequently, they may also have advantageous properties for application in SSBs. However, to date, no such studies have been performed that examine nanosheet-coated CAMs in batteries using superionic solid electrolytes.

Herein, we investigate the coating of polycrystalline LiNi_{0.85}Co_{0.1}Mn_{0.05}O₂ (NCM851005, referred to as NCM in the following) with commercially available nanosheet materials. The focus is on improving the protective properties while avoiding the synthesis of conductive materials, such as graphene. This precautionary measure is taken to mitigate (electro)chemical degradation (oxidation) of the solid electrolyte. We first concentrate on establishing a coating method for hexagonal boron nitride (h-BN), which is isostructural to graphite/graphene, but electronically insulating.^[40] h-BN is attractive as a coating material because of its high chemical stability, reacting only under extreme conditions (e.g., boiling sulfuric acid).^[22] Dry- and liquid-phase deposition routes are compared with regards to coating content and distribution on the particle surface, as well as structural integrity of the CAM. Specifically, h-BN coating is compared to that achieved with WS₂ and exfoliated

((CH₃(CH₂)₃)₄N)₄Nb₆O₁₇. The latter materials are known as functional coatings and can be readily obtained in nanosheet format.^[41–45] WS₂ is found to undergo side reactions with the NCM particles upon mild annealing, and electrochemical testing shows that nanosheet coating leads to stability improvements in SSBs, but not in LIB cells. This highlights the differences in stabilization strategies for batteries with liquid and solid electrolytes and emphasizes the need for further studies.

2. Results and Discussion

2.1. Coating Methods

Liquid-phase stabilization of h-BN (e.g., from liquid-phase exfoliation) can be achieved with similar solvents or solvent-dispersant systems as for graphene.^[42,46,47] Much of the work on h-BN stabilization has been focused on aqueous dispersions.^[46,48] However, water is known to leach lithium from layered Ni-rich oxide CAMs and to adversely affect their surface structure and electrochemical properties (formation of rock salt-type NiO, etc.).^[49,50] Furthermore, the dispersant may decompose and lead to the formation of surface carbonates during the annealing process after coating. Note that hybrid coatings containing carbonate species have recently been shown to have a profound effect on the cycling performance of thiophosphate-based SSBs.^[11,12,51–54] To avoid false interpretation of carbonate coating rather than stabilization induced by the nanosheet materials, we focus on methods that do not rely on aqueous dispersions and organic dispersants.

Dry coating is a facile approach to avoid solvent exposure and dispersant chemistry altogether. Ball milling at a rotational speed of 100 rpm and with small ZrO₂ balls was chosen to limit the energy input. Further exfoliation of the nanosheets may be achieved under ball-milling conditions, since the CAM particles, in principle, can act as an abrasive agent, as reported for the exfoliation of nanosheet materials with common salts.^[55,56] The material obtained was probed using scanning electron microscopy (SEM), see **Figure 1b,g,l** [Figure 1a,f,k is showing the pristine (uncoated) NCM]. Investigation of the surface of the secondary particles revealed the deposition of small circular nanosheets and, in some instances, shearing of individual sheets. This is sometimes observed during exfoliation of individual nanosheets and suggests that low-energy ball milling helps to further increase the available surface by shearing of few-layer sheets.^[57] However, the secondary particle structure was only partially retained, as there was clearly chipping and fracturing of the NCM CAM.

To improve the mixing of nanosheets and NCM and reduce mechanical strain, it was attempted to perform wet milling using acetonitrile (with NCM:acetonitrile = 1:1 by weight). As seen in **Figure 1c,h,m**, this exacerbated the problem of particle disintegration, which may be due to dissolution of residual lithium from the polycrystalline sample. It was also attempted to mechanically mix the materials using a laboratory grade blender (Kinematica), but they tended to stick to the sides of the jar and agglomerate rather than being mixed uniformly. Therefore, although there is some decent deposition, the particle disintegration does not allow employing mechanical mixing for nanosheet coating of polycrystalline CAMs.

While water is detrimental when working with Ni-rich cathodes,^[49] organic solvents may be used to suspend the

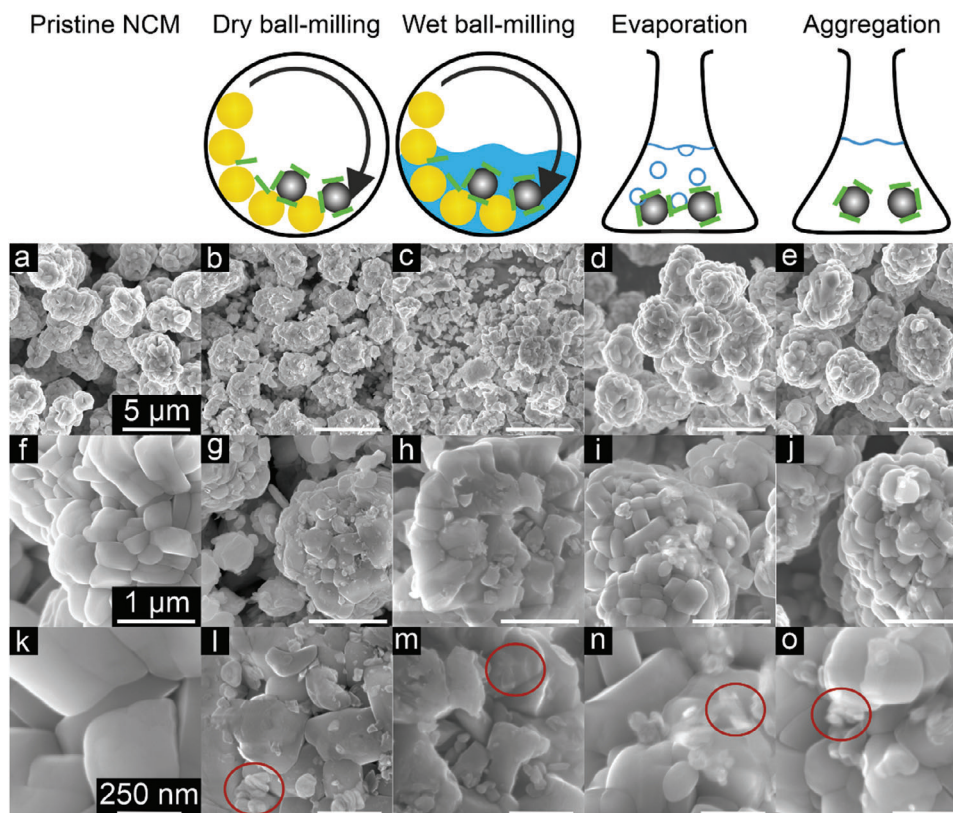


Figure 1. Schematic representation of nanosheet coating by dry ball-milling, wet ball-milling, solvent evaporation and spontaneous adsorption. a–o) Low- and high-magnification SEM images for the comparison of coating attempts using h-BN nanosheets (highlighted by red circles). a, f, k) Uncoated NCM particles, b, g, l) dry ball-milling assisted coating, c, h, m) wet ball-milling assisted coating, d, i, n) solvent evaporation-based coating and e, j, o) spontaneous adsorption-based coating.

nanosheets and deposit them onto the particles. Two methods of attaching nanosheets to the surface were tested, namely evaporation under agitation and spontaneous aggregation. In the first case, 10 mg of h-BN nanosheets were dispersed in 10 mL of acetonitrile via sonication for 30 min, after which 1.0 g of CAM was added. The mixture was then vigorously stirred for 10 min at room temperature, followed by removal of the solvent in vacuo with continuous stirring. In the second approach, the h-BN nanosheets were suspended as described. Afterward, NCM was added, and the mixture was vigorously stirred overnight to allow the nanosheets to spontaneously adhere to the particle surface. The suspension was then left to separate, and the modified CAM was harvested as the sediment. Lastly, the residual solvent was decanted, and the powder was dried again under vacuum. The coated samples were also probed using SEM, as shown in Figure 1d,e,i,j,n,o. As evident, in both samples, the secondary particle structure was retained, and there are no signs of deagglomeration or chipping. Aggregates of nanosheets are clearly visible on the particle surface. However, in the case of “evaporation under agitation”, the nanosheet content appears to be slightly higher. This is also corroborated by the observation that even after stirring overnight the supernatant was still somewhat turbid, indicating that not all of the nanosheets attach to the surface. Furthermore, the evaporation-based processing takes less time, and the sample is exposed to solvent for a shorter duration, which is why this route was used in the following coating experiments.

Taken together, the “evaporation under agitation” approach worked best with this specific set of materials. However, dry coating also yields high loadings (good surface coverage). In addition, the nanosheets appear to attach closely to the particle surface, whereas more fluffy aggregates are formed upon wet processing. For CAM morphologies that have a higher mechanical strength, such as single- or quasi single-crystalline, dry coating may indeed be the better choice, as particle (surface) integrity plays a crucial role in the cyclability.^[58,59] As a preliminary test, we have examined the dry coating of a single-crystalline NCM831205 (83% Ni content). The results indicate that h-BN deposition onto the CAM surface is indeed possible. However, the coating coverage was not very uniform (see Figure S1, Supporting Information), and determining the optimal process parameters would require further study. Nevertheless, dry coating as such seems promising for the emerging single-crystal CAMs, for which surface-based degradation is also a major contributor to capacity fading.^[59]

2.2. Comparison of h-BN, WS₂ and Niobate-Type Nanosheet Coatings

To study a broader range of materials, the “evaporation under agitation” approach discussed above was applied to coating of the NCM CAM with 1 wt.% of h-BN, WS₂ and exfoliated ((CH₃(CH₂)₃)₄N)₄Nb₆O₁₇ nanosheets (hereafter referred to

Table 1. Structural parameters from Rietveld refinement for the uncoated and nanosheet-coated NCMs and corresponding ICP-OES analysis of the coating content.

Sample	NCM	hBN-NCM	WS ₂ -NCM	Nb-NCM
R _{wp} [%]	11.74	10.18	10.63	8.75
R _{Bragg} [%]	1.67	1.51	1.39	1.47
V [Å ³]	101.01(1)	101.04(1)	101.05(6)	101.32(2)
a [Å]	2.8682(1)	2.8683(6)	2.8687(1)	2.8712(1)
c [Å]	14.1770(9)	14.1782(12)	14.1787(10)	14.1897(12)

Sample	hBN-NCM	WS ₂ -NCM	Nb-NCM
Probed element	B	W	Nb
Assumed stoichiometry	BN	WS ₂	Nb ₆ O ₁₇ ⁴⁻
Coating content [wt.%]	0.45(6)	1.11(2)	0.91(3)

as hBN-NCM, WS₂-NCM and Nb-NCM, respectively). For ensuring good contact with the secondary particle structure, the samples were heated at 400 °C in oxygen, which has been shown previously to be an optimal post-deposition treatment temperature for oxide coatings^[10,19,20] in thiophosphate-based SSB cells. The organic cation in ((CH₃(CH₂)₃)₄N)₄Nb₆O₁₇ decomposes during heating, yielding some kind of lithiated niobate-type (Li_xNbO_y) coating.^[60]

The hBN-NCM, WS₂-NCM and Nb-NCM samples were investigated by SEM, inductively coupled plasma-optical emission spectroscopy (ICP-OES) and powder X-ray diffraction (PXRD), as shown in Table 1 and Figure 2a–h. The pristine NCM as a reference was treated under the same conditions as the other samples, but in absence of nanosheets. Structural analysis indicated that all materials are single phase and the lattice parameters do not change much with coating. Exemplary PXRD patterns collected from WS₂-NCM and hBN-NCM and Rietveld fits to the patterns are shown in Figure S2 (Supporting Information). The greatest difference to the reference CAM was found for Nb-NCM, which exhibits slightly larger lattice parameters and unit-cell volume. This could point toward structural degradation, since an increase in lattice parameters is typically associated with the formation of Ni_{Li}⁺ point defects (cation intermixing). This, in turn, may be due to lithium loss from the NCM and possibly “absorption” by the niobate-type coating. ICP-OES revealed that the coating content is lowest for h-BN, with only about half of the nominal amount deposited onto the CAM particles. However, for both WS₂-NCM and Nb-NCM, it was close to the targeted content, indicating effective coating (note: 0.91 wt.% would theoretically correspond to 0.97 wt.% LiNbO₃). For the WS₂ nanosheets, it was even higher than the targeted loading, which may be because of the presence of oxygen impurities, as the nanosheets can readily oxidize at room temperature. In such a case, the actual stoichiometry to be considered would be WS_{2-x}O_x, causing excessive tungsten content when aiming for 1 wt.% WS₂ coating due to the lower molecular weight. The low- and high-magnification SEM images in Figure 2c–h confirm successful deposition of nanosheets onto the surface of the secondary particles, with hBN having a relatively lower affinity to the CAM. As expected, the different nanosheet materials were attached in a surface-parallel manner.

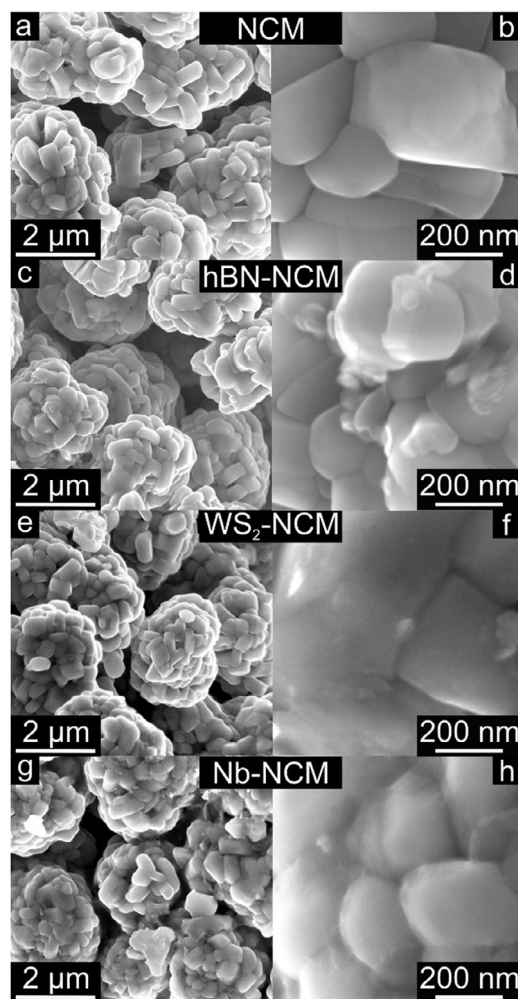


Figure 2. SEM images at different magnifications of a,b) uncoated NCM, c,d) hBN-NCM, e,f) WS₂-NCM and g,h) Nb-NCM.

2.3. Electrochemical Testing in Battery Cells

The electrochemical properties of the uncoated and nanosheet-coated NCM samples were evaluated in LIB half-cells and pellet-stack SSB cells. With regards to the cells with LP57 electrolyte, the tests were conducted in the potential window of 3.0–4.3 V versus Li⁺/Li at a constant temperature of 25 °C and at C-rates ranging from C/10 to 10C. The first-cycle charge/discharge curves at C/10 were similar for the different CAMs, as can be seen from Figure 3a, suggesting that surface coating has no notable effect on the original NCM structure/morphology. In addition, except for Nb-NCM ($q_{\text{dis}} = 195 \text{ mAh g}^{-1}$), all cells delivered a similar first-cycle specific discharge capacity of $q_{\text{dis}} = 208 (\pm 2) \text{ mAh g}^{-1}$. As indicated by PXRD analysis, this observation may be attributed to a larger fraction of nickel substitutional defects in Nb-NCM due to formation of lithium niobate during post-deposition anneal. It should be noted that the latter may also add to the cell resistance (impedance buildup).^[60]

Unlike LIBs, the SSB cells with argyrodite Li₆PS₅Cl (referred to as LPSCl) electrolyte were tested at 45 °C in a potential range between 2.28 and 3.68 V versus In/InLi ($\approx 2.9\text{--}4.3 \text{ V vs Li}^+/\text{Li}$). As

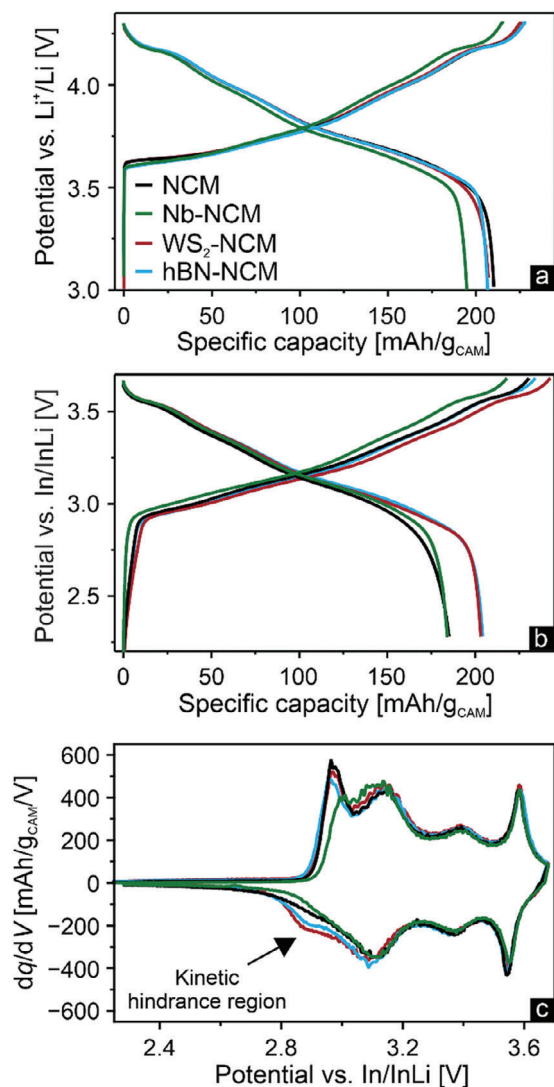


Figure 3. First-cycle charge/discharge curves of the uncoated and nanosheet-coated NCM CAMs a) in LIB half-cells with LP57 electrolyte and b) in SSB cells with LPSCl electrolyte at a rate of C/10. c) Differential capacity curves of the cells shown in b). For each material, three (LIB) or two cells (SSB) were tested and the data averaged.

expected based on the LIB data, the different CAMs revealed similar electrochemical behaviors in the initial cycle at C/10 rate (see Figure 3b). Except for Nb-NCM ($q_{\text{dis}} = 184 \text{ mAh g}^{-1}$), the coated samples achieved a higher initial specific discharge capacity than the uncoated NCM [$q_{\text{dis}} = 204 (\pm 1) \text{ mAh g}^{-1}$ vs 185 mAh g^{-1}]. As shown in Figure 2c–h, the nanosheets did not fully cover the particle surface, especially when considering areas where the primary grains meet, resulting in a somewhat non-uniform coating. When tested in LIBs, liquid electrolyte can easily access the exposed surfaces and penetrate into microcracks, leading to minor or even no improvements in cycling performance (see also Figure S3, Supporting Information). By contrast, when tested in SSBs, the coatings strongly reduce the contact area between the bare CAM and the LPSCl electrolyte, which helps to prevent interfacial side reactions from occurring, and therefore positively affects cyclability.

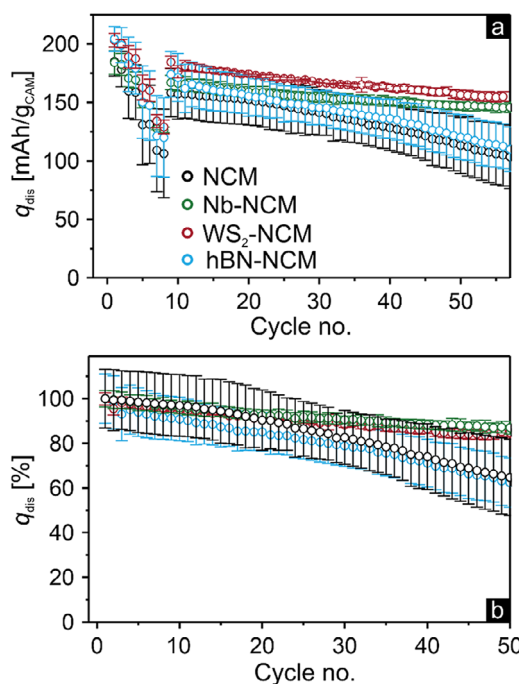


Figure 4. Cyclability of uncoated and nanosheet-coated NCM CAMs in SSB cells with LPSCl electrolyte. a) Rate performance testing with two cycles each at C/10, C/5, C/2 and 1C, followed by 50 cycles at C/5. b) Relative stability (capacity retention) with 100% referring to the first cycle at C/5 after the rate capability test. The error bars represent the standard deviation from two independent cells.

Differential capacity plots can provide thorough information about the phase transitions occurring during cycling. As seen from Figure 3c, the only difference between the uncoated and WS_2 /h-BN nanosheet-coated samples is an additional feature at the end of discharge (at $\approx 2.9 \text{ V}$ vs In/InLi). This is commonly referred to as the so-called “kinetic hindrance” region, and is more apparent for Ni-rich CAMs exhibiting a high lithium diffusivity (e.g., because of low Ni_{Li}^* defect concentration or cycling at elevated temperatures).^[61–63] However, in the present work, the primary particle (grain) size and defect concentration are similar for the different materials tested. The same holds for the temperature during cycling. This leaves the protective coating as a reason for the facilitated lithium diffusion (by preventing unfavorable side reactions and impedance buildup during cycling). Additional features that may originate from redox activity and/or degradation of the nanosheets upon battery operation were not observed. By contrast, Nb-NCM revealed smaller peaks, which is indicative of a different mechanism of improved capacity retention and further agrees with the lower specific capacity compared to the uncoated NCM.

Figure 4a shows the cyclability of the uncoated and nanosheet-coated NCM CAMs in SSB cells at different C-rates. In agreement with the results from SEM imaging and ICP-OES analysis regarding surface coverage, WS_2 -NCM and Nb-NCM exhibited much improved cycling performance and relative stability (see Figure 4b; Figure S4, Supporting Information). After 50 cycles at C/5, hBN-NCM, WS_2 -NCM and Nb-NCM showed capacity retentions of 63%, 85% and 87%, respectively, compared to

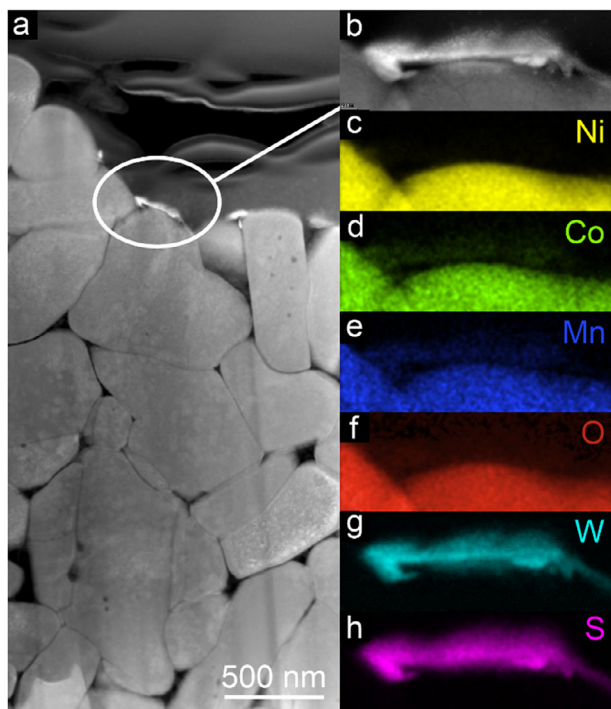


Figure 5. EDS analysis of FIB-cut WS_2 -NCM with a) overview and b) zoomed-in HAADF STEM images and c–h) corresponding elemental maps from EDS analysis.

64% for the uncoated CAM. Interestingly, the niobate-type coating also resulted in increased Coulomb efficiency, from 80% for the uncoated material to 85% for Nb-NCM, in the initial cycle (see Figure 3b). As mentioned previously, residual lithium is probably being consumed to some degree by the nanosheets during post-processing in the formation of Li_xNbO_y , which itself is a well-established coating material in LIBs and SSBs.^[45] For that reason, this kind of coating will be investigated in more detail in the future.

Overall, protective nanosheet coatings impart stabilization to the cathode interface in thiophosphate-based cells, thus achieving relatively similar levels of effectiveness to state-of-the-art coating materials and techniques.^[11,16–20] However, it remains to be seen if they will be capable of outperforming tailored sol-gel or ALD coatings, which may find application in future generations of bulk-type SSBs.

2.4. Analysis of WS_2 -NCM

From the electrochemical testing, WS_2 -NCM was found to deliver the highest specific capacities (note: similar stabilization was achieved with the niobate-type nanosheets in SSB cells). Since WS_2 is reactive toward ambient oxygen,^[64–67] it is necessary to characterize the actual coating species given that the nanosheets may transform into some oxidized state during deposition and/or post-deposition anneal.

Figure 5a–h shows results from high-angle annular dark-field scanning transmission electron microscopy (HAADF STEM) and energy-dispersive X-ray spectroscopy (EDS) of a focused ion beam (FIB)-cut lamella of the WS_2 -NCM sample. HAADF

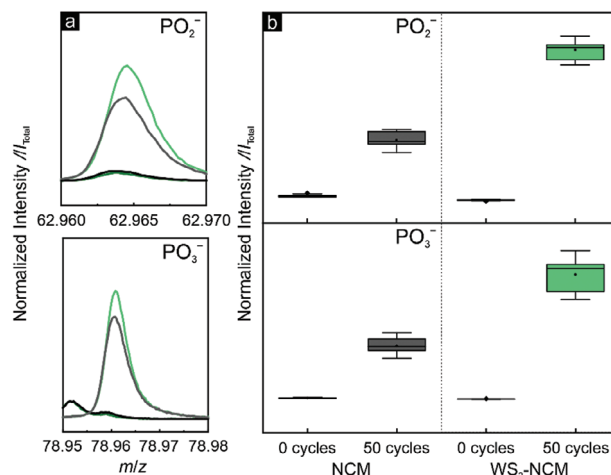


Figure 6. ToF-SIMS data for fragments (PO_2^- and PO_3^-) characteristic of interfacial degradation products. a) Representative mass spectra collected from the uncoated NCM and WS_2 -NCM composite cathodes before and after cycling. b) Corresponding boxplots of normalized intensities containing ten data points each.

STEM imaging (see Figure 5a) indicated sparse distribution of nanosheets on the particle (apparent from the large differences in contrast). Upon closer inspection (see Figure 5b), the nanosheets were found to not perfectly follow the curvature of the substrate, unlike conformal coatings, but instead they seem to have relatively loose contact with the CAM surface. Despite post-annealing in oxygen, WO_3 formation was not clearly recognizable from the EDS maps presented in Figure 5c–h. However, some minor oxygen signal appeared in the area of the nanosheet coating, which points toward partial WS_2 oxidation. Apart from that, when probing other areas of the particle surface using fast Fourier transform (FFT) analysis of TEM lattice fringes (see Figure S5, Supporting Information), some of the reflections matched with the tetragonal WO_3 phase, thus confirming oxidation of WS_2 .

To further elucidate the interfacial stabilization mechanism, the uncoated NCM and WS_2 -NCM composite cathodes—before and after 50 cycles in SSB cells—were studied by time-of-flight secondary ion mass spectrometry (ToF-SIMS). Surface analysis via ToF-SIMS enables the detection of decomposition products, such as phosphates and sulfates, which has been described in detail by Walther and coworkers.^[5,36,68] Because the WS_2 coating contains sulfur, the analysis of sulfate/sulfite fragments can lead to misinterpretation of data, and therefore they were not considered. Representative mass spectra collected before and after cycling are shown in Figure 6a. To ensure good statistics and data reliability, 10 mass spectra per sample were measured and summarized in box plots (see Figure 6b). As evident, the amount of PO_x^- fragments (PO_2^- and PO_3^-) after 50 cycles was significantly higher for WS_2 -NCM compared to the uncoated sample. This result is somewhat surprising and not in apparent agreement with the cycling performance in Figure 4, showing that uncoated NCM suffers from much faster capacity fading than the coated counterpart. Rather, the data suggest that the decomposition interphase [similar to the cathode electrolyte interphase (CEI) in liquid-electrolyte-based batteries], which is formed by side reactions at the interface between the NCM (oxygen source)

and the LPSCl (phosphorus source), is not necessarily detrimental to the cyclability of the thiophosphate-based SSBs. A possible explanation for this finding may be that the decomposition interphase exhibits favorable transport properties, especially with regards to partial ionic conductivity. According to Homma et al.,^[69] the ionic conductivity of a mixture of different materials depends on the actual composition. Consequently, it can be inferred that the coating directly affects the mixing ratio of degradation products and/or WS_2 catalyzes the formation of other species. Additionally, a signal of low intensity appeared at $m/z = 78.96$ in the pristine state. This feature has been previously linked to the presence of PSO^- fragments.^[5] Upon cycling, the electrolyte undergoes some (electro)chemical degradation, accompanied by the formation of oxygenated sulfur and phosphorus species, among others. The reliability of the presented data (i.e., trend in signal intensities) was also verified by another normalization technique (see Figure S6, Supporting Information). In this case, the intensities were not normalized to the total ion signal, but rather to the NiO_2^- fragment, the latter representing the NCM.

The results hint at an underlying stabilization mechanism that is distinct from the classical “inert” cathode interface/interphase associated with oxide nanocoatings.^[12] Another explanation that would be consistent with the observations would be mitigation of transition-metal dissolution, as proposed by Maiti et al. for WSe_2 coating (LIB application).^[29] Indeed, leaching is not limited to liquid electrolytes, but has also been reported recently for thiophosphate-based SSBs.^[70] Regardless, higher surface coverage of the NCM particles would likely help to unravel the mechanism more easily. However, in this work, we were limited to partial surface coverage due to mechanical stability issues of the CAM secondary particles, as discussed above. Nevertheless, these relatively poorly coated materials demonstrated substantial improvements in cycling performance, which renders the tailoring of nanosheet coatings, e.g. by focusing on mechanically more robust single-crystalline CAMs, all the more intriguing.

3. Conclusion

Lithium thiophosphate solid electrolytes are promising superionic materials for use in solid-state batteries owing to their high room-temperature ionic conductivity that is readily accessible by cold-pressing. However, their enhanced reactivity toward oxidation necessitates the application of protective coatings to stabilize the cathode/electrolyte interface. Here, we have examined whether nanosheet materials lend themselves as protective coating agents in liquid- and solid-electrolyte-based lithium-ion batteries. First, we have evaluated various coating methods and found that deposition from dispersions in organic solvents is best suited for surface modification without harming the cathode active material. Next, we have compared different kinds of nanosheets in conventional and solid-state batteries. Our findings demonstrate that significant stabilization through nanosheet coating can only be achieved in thiophosphate-based solid-state cells, which is likely related to the relative immobility of the solid electrolyte when compared to organic liquid electrolytes. However, for the chemically inert coating, h-BN, no stabilization was observed, while the “more reactive” coatings, WS_2 and Li_xNbO_y , had a major effect on cycling performance. Overall, the concept of nanosheet coating may be a promising addition to

established surface-modification strategies, especially in the context of solid-state batteries. Nevertheless, the main challenge that needs to be addressed is achieving uniform and conformal surface coverage.

4. Experimental Section

Coating Procedure: The CAM was received from BASF SE (NCM851005, $d_{50} \approx 4 \mu\text{m}$) and the coating materials, h-BN (90 nm) and WS_2 (200 nm), from Sigma-Aldrich as commercial products. The latter materials were used without further processing, while the niobate-type nanosheets were synthesized in house. 10 mg (in case of Nb, for $[K_{4-x}H_xNb_6O_{17}]$) of nanosheet precursor was weighed into 10 mL of dry isopropanol (WS_2 , h-BN) or dry ethanol (Nb) and sonicated for 30 min in an ultrasonication bath. To this mixture, 1 g of CAM was added, followed by stirring for 10 min, after which the solvent was removed under vacuum with continuous agitation. The obtained powders were calcined in a tube furnace under flowing oxygen atmosphere (two atmosphere exchanges per hour) at 400 °C for 1 h and then sieved using a 32 μm stainless steel mesh.

Preparation of $((CH_3(CH_2)_3)_4N)_4Nb_6O_{17}$: First, bulk $K_4Nb_6O_{17} \cdot 3H_2O$ was prepared by a solid-state method, in which Nb_2O_5 and K_2CO_3 (2:3 molar ratio) were ground and heated at 1100 °C for 10 h.^[71,72] The material was then subject to ion exchange (K^+ to H^+) by stirring 3.0 g of $K_4Nb_6O_{17} \cdot 3H_2O$ in 150 mL of 0.2 mol L^{-1} H_2SO_4 for 3 days. Next, the solid was filtered, washed with water and dried at 70 °C. The nanosheets were obtained by exfoliation of bulk $K_{4-x}H_xNb_6O_{17}$ (0.5 g) using 100 mL of $8 \cdot 10^{-3}$ mol L^{-1} tetrabutylammonium hydroxide for 7 days (see Figure S7, Supporting Information).^[73,74] Once the stirring is suspended, the non-exfoliated material tends to precipitate out, while the exfoliated layers remain in the form of a stable suspension. The suspension of nanosheets was collected, followed by drying at 70 °C.

Microscopy: SEM imaging of the as-prepared samples was performed using a LEO-1530 microscope (Carl Zeiss AG). TEM was performed on a Themis Z (Thermo Fisher Scientific) double-corrected transmission electron microscope operated at an acceleration voltage of 300 kV. Lift-out samples were prepared on a STRATA (FEI) dual-beam system equipped with a gallium-ion source. The samples were milled at 30 kV, followed by final polishing at 2 kV to reduce surface damage. Prior to milling, the sample surface was protected by deposition of a carbon layer. STEM images were recorded using a HAADF detector. Elemental analysis was performed by EDS employing a Super-X detector. JEMS software was used to index the FFT patterns. The TEM image presented in Figure S7 (Supporting Information) was acquired on a Tecnai G2 F20 TMP equipped with a field emission gun operating at 200 kV (featuring TWIN objective lenses and a point resolution of 0.27 nm).

Powder XRD and Pattern Refinement: XRD data were collected from powder samples in 0.03 mm glass capillaries (Hilgenberg) on a STADI P (STOE) diffractometer in Debye–Scherrer geometry with monochromatic $Mo-K_{\alpha 1}$ radiation ($\lambda = 0.7093 \text{ \AA}$, 50 kV, and 40 mA) and a Mythen 1K detector (DECTRIS). The different datasets were analyzed using TOPAS Academic V7. First, Le Bail fitting was done (Chebyshev polynomial with 10 terms for background correction); lattice parameters, zero-shift, axial divergence and crystallite size were extracted as Gaussian and Lorentzian contributions. The results of the Le Bail analysis were used as initial parameters for Rietveld refinement, during which the site occupancies, Debye–Waller factors and oxygen coordinates were refined in parallel until convergence was achieved.

Chemical Analysis: ICP-OES measurements were conducted using a Thermo Fisher Scientific ICP 7600 DUO. The CAMs were dissolved in an acid digester using a graphite furnace. Mass fractions were obtained from three independent measurements per sample. About 10 mg of material was dissolved in a mixture of hydrochloric acid and nitric acid at 353 K for 4 h. The digested samples were diluted prior to analysis, which was done with four different calibration solutions and an internal standard (Sc). The concentration range of the calibration solutions did not exceed a decade.

Two or three wavelengths of each element were used for quantitative analysis.

Electrochemical Testing: The sieved CAMs were mixed with Super C65 carbon black additive and polyvinylidene difluoride binder (PVDF, Solef 5130, Solvay) in a ratio of 94:3:3 by weight and cast onto a 0.03 mm-thick aluminum foil using an Erichsen Coatmaster 510 film applicator (140 μm slit thickness of the stainless-steel doctor blade). The electrodes were dried under vacuum at 120 °C for at least 10 h, calendared at 14 N mm⁻¹ (Sumet Messtechnik) and cut into circular 13 mm-diameter discs. LIB coin cells were assembled using the cathodes, a glass fiber GF/D separator, LP57 electrolyte (1 M LiPF₆ in a 3:7 mixture of ethylene carbonate and ethyl methyl carbonate) and a lithium-metal anode in an Ar-filled glovebox with a crimping pressure of 1 t. The uncoated and coated CAMs (≈10 mg cm⁻² areal loading) were tested electrochemically at 25 °C and at C-rates ranging from C/10 to 10C (with 1C = 190 mA g⁻¹).

SSB cells were assembled according to a previously described procedure.^[10] For the cathode, 10–12 mg of a composite containing 69 wt.% CAM (≈10 mg cm⁻² areal loading), 1 wt.% Super C65 and 30 wt.% LPSCl solid electrolyte was used. LPSCl (100 mg) and In/InLi were used as separator and anode, respectively. InLi alloy was prepared in situ by pressing In and Li foils together, with the In foil initially facing the separator layer. The cells were cycled under constant current mode at 45 °C while maintaining a uniaxial stack pressure of 81 MPa. An initial rate test of five cycles at C/10, C/5, C/2 and 1C was followed by 50 cycles at C/5.

SIMS Analysis: ToF-SIMS was conducted using a M6 Hybrid SIMS (IONTOF GmbH) equipped with a 30 kV Bi-cluster primary ion gun for analysis. In general, during ToF-SIMS measurements, charged fragments are obtained as a result of a collision cascade that results from the impact of the high-energy primary ion beam. All samples were prepared in the same way and under the same conditions in a glovebox, attached to the sample holder using non-conductive adhesive tape and transferred to the instrument using the LEICA EM VCT500 shuttle (Leica Microsystems). Accordingly, composite cathodes with WS₂-coated NCM were compared to those using uncoated material. The samples were analyzed before and after cycling. To probe the interfaces in the composite cathodes, the current collector was removed. The instrument was operated in spectrometry mode using Bi₃⁺ as primary ions (0.60 pA) in negative mode, providing high mass resolution [FWHM $m/\Delta m > 13\,000$ @ $m/z = 62.97$ (PO₂⁻)]. The analysis area was set to 100 · 100 μm², which was rasterized with 128 · 128 pixels and a primary ion dose of 1.0 · 10¹² ions cm⁻². To ensure data reliability, 10 mass spectra were measured per sample. Evaluation of the ToF-SIMS data was done with the software SurfaceLab 7.2 (IONTOF GmbH).

Supporting Information

Supporting Information is available from the Wiley Online Library or from the author.

Acknowledgements

This work was partly supported by BASF SE. The authors are grateful to the Federal Ministry of Education and Research (Bundesministerium für Bildung und Forschung, BMBF) for funding within the projects SUS-TRAB (03XP0415D) and FestBatt (03XP0430A, 03XP0433D). The authors acknowledge the support from the Karlsruhe Nano Micro Facility (KNMFi, www.knmf.kit.edu), a Helmholtz research infrastructure at Karlsruhe Institute of Technology (KIT, www.kit.edu). The authors also thank Thomas Bergfeldt and team for conducting the ICP-OES analysis, Matteo Bianchini for helpful discussions and the Laboratory of Nano and Quantum Engineering (LNQE, Leibniz University Hannover) for collecting the TEM imaging data in Figure S7 (Supporting Information).

Open access funding enabled and organized by Projekt DEAL.

Conflict of Interest

The authors declare no conflict of interest.

Data Availability Statement

The data that support the findings of this study are available from the corresponding author upon reasonable request.

Keywords

interface stability, layered Ni-rich cathode, lithium-ion battery, nanosheet coating, solid-state battery

Received: December 16, 2023

Revised: March 3, 2024

Published online:

- [1] J. Janek, W. G. Zeier, *Nat. Energy* **2016**, *1*, 16141.
- [2] Y. Yusim, E. Trevisanello, R. Ruess, F. H. Richter, A. Mayer, D. Bresser, S. Passerini, J. Janek, A. Henss, *Angew. Chem., Int. Ed.* **2023**, *62*, e202218316.
- [3] J. Janek, W. G. Zeier, *Nat. Energy* **2023**, *8*, 230.
- [4] F. P. McGrogan, T. Swamy, S. R. Bishop, E. Eggleton, L. Porz, X. Chen, Y.-M. Chiang, K. J. Van Vliet, *Adv. Energy Mater.* **2017**, *7*, 1602011.
- [5] F. Walther, R. Koerver, T. Fuchs, S. Ohno, J. Sann, M. Rohnke, W. G. Zeier, J. Janek, *Chem. Mater.* **2019**, *31*, 3745.
- [6] S. P. Culver, R. Koerver, W. G. Zeier, J. Janek, *Adv. Energy Mater.* **2019**, *9*, 1900626.
- [7] P. Minnmann, F. Strauss, A. Bielefeld, R. Ruess, P. Adelhelm, S. Burkhardt, S. L. Dreyer, E. Trevisanello, H. Ehrenberg, T. Brezesinski, F. H. Richter, J. Janek, *Adv. Energy Mater.* **2022**, *12*, 2201425.
- [8] B.-X. Shi, Y. Yusim, S. Sen, T. Demuth, R. Ruess, K. Volz, A. Henss, F. H. Richter, *Adv. Energy Mater.* **2023**, *13*, 2300310.
- [9] Y. Ma, J. H. Teo, D. Kitsche, T. Diemant, F. Strauss, Y. Ma, D. Goonetilleke, J. Janek, M. Bianchini, T. Brezesinski, *ACS Energy Lett.* **2021**, *6*, 3020.
- [10] D. Kitsche, F. Strauss, Y. Tang, N. Bartnick, A.-Y. Kim, Y. Ma, C. Kübel, J. Janek, T. Brezesinski, *Batter. Supercaps* **2022**, *5*, e202100397.
- [11] S. Payandeh, F. Strauss, A. Mazilkin, A. Kondrakov, T. Brezesinski, *Nano Res. Energy* **2022**, *1*, e9120016.
- [12] A.-Y. Kim, F. Strauss, T. Bartsch, J. H. Teo, T. Hatsukade, A. Mazilkin, J. Janek, P. Hartmann, T. Brezesinski, *Chem. Mater.* **2019**, *31*, 9664.
- [13] K. Takada, N. Ohta, L. Zhang, K. Fukuda, I. Sakaguchi, R. Ma, M. Osada, T. Sasaki, *Solid State Ionics* **2008**, *179*, 1333.
- [14] G. Oh, M. Hirayama, O. Kwon, K. Suzuki, R. Kanno, *Chem. Mater.* **2016**, *28*, 2634.
- [15] R. S. Negi, Y. Yusim, R. Pan, S. Ahmed, K. Volz, R. Takata, F. Schmidt, A. Henss, M. T. Elm, *Adv. Mater. Interfaces* **2022**, *9*, 2101428.
- [16] Y. Ma, R. Zhang, Y. Tang, Y. Ma, J. H. Teo, T. Diemant, D. Goonetilleke, J. Janek, M. Bianchini, A. Kondrakov, T. Brezesinski, *ACS Nano* **2022**, *16*, 18682.
- [17] Y. Ma, J. H. Teo, F. Walther, Y. Ma, R. Zhang, A. Mazilkin, Y. Tang, D. Goonetilleke, J. Janek, M. Bianchini, T. Brezesinski, *Adv. Funct. Mater.* **2022**, *32*, 2111829.
- [18] R. Zhang, Y. Ma, Y. Tang, D. Goonetilleke, T. Diemant, J. Janek, A. Kondrakov, T. Brezesinski, *Chem. Mater.* **2023**, *35*, 6835.
- [19] D. Kitsche, Y. Tang, Y. Ma, D. Goonetilleke, J. Sann, F. Walther, M. Bianchini, J. Janek, T. Brezesinski, *ACS Appl. Energy Mater.* **2021**, *4*, 7338.
- [20] D. Kitsche, Y. Tang, H. Hemmelmann, F. Walther, M. Bianchini, A. Kondrakov, J. Janek, T. Brezesinski, *Small Sci.* **2023**, *3*, 2200073.
- [21] C. Lee, X. Wei, J. W. Kysar, J. Hone, *Science* **2008**, *321*, 385.
- [22] N. I. Kovtyukhova, Y. Wang, R. Lv, M. Terrones, V. H. Crespi, T. E. Mallouk, *J. Am. Chem. Soc.* **2013**, *135*, 8372.

- [23] S. Hu, M. Lozada-Hidalgo, F. C. Wang, A. Mishchenko, F. Schedin, R. R. Nair, E. W. Hill, D. W. Boukhvalov, M. I. Katsnelson, R. A. W. Dryfe, I. V. Grigorieva, H. A. Wu, A. K. Geim, *Nature* **2014**, 516, 227.
- [24] Y. Huang, J. Wu, K. C. Hwang, *Phys. Rev. B* **2006**, 74, 245413.
- [25] C. Backes, R. J. Smith, N. McEvoy, N. C. Berner, D. McCloskey, H. C. Nerl, A. O'Neill, P. J. King, T. Higgins, D. Hanlon, N. Scheuschner, J. Maultzsch, L. Houben, G. S. Duesberg, J. F. Donegan, V. Nicolosi, J. N. Coleman, *Nat. Commun.* **2014**, 5, 4576.
- [26] K.-Y. Park, J.-M. Lim, N. S. Luu, J. R. Downing, S. G. Wallace, L. E. Chaney, H. Yoo, W. J. Hyun, H.-U. Kim, M. C. Hersam, *Adv. Energy Mater.* **2020**, 10, 2001216.
- [27] K.-Y. Park, Y. Zhu, C. G. Torres-Castanedo, H. J. Jung, N. S. Luu, O. Kahvecioglu, Y. Yoo, J.-W. T. Seo, J. R. Downing, H.-D. Lim, M. J. Bedzyk, C. Wolverton, M. C. Hersam, *Adv. Mater.* **2022**, 34, 2106402.
- [28] P. Xiao, Y. Cao, W. Li, G. Li, Y. Yu, Z. Dai, Z. Du, X. Chen, J. Sun, W. Yang, *ACS Appl. Mater. Interfaces* **2021**, 13, 29714.
- [29] S. Maiti, R. Konar, H. Sclar, J. Grinblat, M. Talianker, M. Tkachev, X. Wu, A. Kondrakov, G. D. Nessim, D. Aurbach, *ACS Energy Lett.* **2022**, 7, 1383.
- [30] R. Rojasee, R. Shahbazian-Yassar, *ACS Nano* **2020**, 14, 2628.
- [31] S. Sharifi-Asl, F. A. Soto, T. Foroozan, M. Asadi, Y. Yuan, R. Deivanayagam, R. Rojasee, B. Song, X. Bi, K. Amine, J. Lu, A. Salehikhajin, P. B. Balbuena, R. Shahbazian-Yassar, *Adv. Funct. Mater.* **2019**, 29, 1901110.
- [32] Y. Shi, S.-L. Chou, J.-Z. Wang, D. Wexler, H.-J. Li, H.-K. Liu, Y. Wu, *J. Mater. Chem.* **2012**, 22, 16465.
- [33] M. A. Razmjoo Kholari, P. Paknahad, M. Ghorbanzadeh, *New J. Chem.* **2019**, 43, 2766.
- [34] J.-H. Shim, Y.-M. Kim, M. Park, J. Kim, S. Lee, *ACS Appl. Mater. Interfaces* **2017**, 9, 18720.
- [35] C. W. Park, J.-H. Lee, J. K. Seo, W. Y. Jo, D. Whang, S. M. Hwang, Y.-J. Kim, *Nat. Commun.* **2021**, 12, 2145.
- [36] F. Walther, F. Strauss, X. Wu, B. Mogwitz, J. Hertle, J. Sann, M. Rohnke, T. Brezesinski, J. Janek, *Chem. Mater.* **2021**, 33, 2110.
- [37] T. Bartsch, F. Strauss, T. Hatsukade, A. Schiele, A.-Y. Kim, P. Hartmann, J. Janek, T. Brezesinski, *ACS Energy Lett.* **2018**, 3, 2539.
- [38] W. Liu, F. Gao, Y. Zang, J. Qu, J. Xu, S. Ji, Y. Huo, J. Qiu, *J. Alloys Compd.* **2021**, 867, 159079.
- [39] S. She, Y. Zhou, Z. Hong, Y. Huang, Y. Wu, *ACS Omega* **2022**, 7, 24851.
- [40] G. Cassabois, P. Valvin, B. Gil, *Nat. Photonics* **2016**, 10, 262.
- [41] D. Becker, M. Börner, R. Nölle, M. Diehl, S. Klein, U. Rodehorst, R. Schmich, M. Winter, T. Placke, *ACS Appl. Mater. Interfaces* **2019**, 11, 18404.
- [42] C. Backes, B. M. Szydłowska, A. Harvey, S. Yuan, V. Vega-Mayoral, B. R. Davies, P.-I. Zhao, D. Hanlon, E. J. G. Santos, M. I. Katsnelson, W. J. Blau, C. Gadermaier, J. N. Coleman, *ACS Nano* **2016**, 10, 1589.
- [43] S.-J. Sim, S.-H. Lee, B.-S. Jin, H.-S. Kim, *J. Power Sources* **2021**, 481, 229037.
- [44] C. Nico, T. Monteiro, M. P. F. Graça, *Prog. Mater. Sci.* **2016**, 80, 1.
- [45] B. N. Nunes, W. van den Bergh, F. Strauss, A. Kondrakov, J. Janek, T. Brezesinski, *Inorg. Chem. Front.* **2023**, 10, 7126.
- [46] C. Backes, T. M. Higgins, A. Kelly, C. Boland, A. Harvey, D. Hanlon, J. N. Coleman, *Chem. Mater.* **2017**, 29, 243.
- [47] R. J. Smith, P. J. King, M. Lotya, C. Wirtz, U. Khan, S. De, A. O'Neill, G. S. Duesberg, J. C. Grunlan, G. Moriarty, J. Chen, J. Wang, A. I. Minett, V. Nicolosi, J. N. Coleman, *Adv. Mater.* **2011**, 23, 3944.
- [48] A. Griffin, A. Harvey, B. Cunningham, D. Scullion, T. Tian, C.-J. Shih, M. Gruening, J. F. Donegan, E. J. G. Santos, C. Backes, J. N. Coleman, *Chem. Mater.* **2018**, 30, 1998.
- [49] D. Pritzl, T. Teufel, A. T. S. Freiberg, B. Strehle, J. Sicklinger, H. Sommer, P. Hartmann, H. A. Gasteiger, *J. Electrochem. Soc.* **2019**, 166, A4056.
- [50] J. Sicklinger, M. Metzger, H. Beyer, D. Pritzl, H. A. Gasteiger, *J. Electrochem. Soc.* **2019**, 166, A2322.
- [51] H. Visbal, S. Fujiki, Y. Aihara, T. Watanabe, Y. Park, S. Doo, *J. Power Sources* **2014**, 269, 396.
- [52] F. Strauss, S. Payandeh, A. Kondrakov, T. Brezesinski, *Mater. Futures* **2022**, 1, 023501.
- [53] S. H. Jung, K. Oh, Y. J. Nam, D. Y. Oh, P. Brüner, K. Kang, Y. S. Jung, *Chem. Mater.* **2018**, 30, 8190.
- [54] F. Strauss, J. H. Teo, J. Maibach, A.-Y. Kim, A. Mazilkin, J. Janek, T. Brezesinski, *ACS Appl. Mater. Interfaces* **2020**, 12, 57146.
- [55] O. Y. Posudievsky, O. A. Khazieieva, V. G. Koshechko, V. D. Pokhodenko, *Theor. Exp. Chem.* **2014**, 50, 103.
- [56] O. Y. Posudievsky, O. A. Khazieieva, V. V. Cherepanov, G. I. Dovbeshko, A. G. Shkavro, V. G. Koshechko, V. D. Pokhodenko, *J. Mater. Chem. C* **2013**, 1, 6411.
- [57] K. R. Paton, E. Varra, C. Backes, R. J. Smith, U. Khan, A. O'Neill, C. Boland, M. Lotya, O. M. Istrate, P. King, T. Higgins, S. Barwich, P. May, P. Puczkarski, I. Ahmed, M. Moebius, H. Pettersson, E. Long, J. Coelho, S. E. O'Brien, E. K. McGuire, B. M. Sanchez, G. S. Duesberg, N. McEvoy, T. J. Pennycook, C. Downing, A. Crossley, V. Nicolosi, J. N. Coleman, *Nat. Mater.* **2014**, 13, 624.
- [58] H.-H. Ryu, B. Namkoong, J.-H. Kim, I. Belharouak, C. S. Yoon, Y.-K. Sun, *ACS Energy Lett.* **2021**, 6, 2726.
- [59] W. van den Bergh, L. Karger, S. Murugan, J. Janek, A. Kondrakov, T. Brezesinski, *ChemElectroChem* **2023**, 10, 202300165.
- [60] Y. Kobayashi, H. Hata, T. E. Mallouk, *MRS Online Proc. Libr.* **2007**, 988, 9880320.
- [61] L. Karger, D. Weber, D. Goonetilleke, A. Mazilkin, H. Li, R. Zhang, Y. Ma, S. Indris, A. Kondrakov, J. Janek, T. Brezesinski, *Chem. Mater.* **2023**, 35, 648.
- [62] L. Karger, S. Korneychuk, W. van den Bergh, S. L. Dreyer, R. Zhang, A. Kondrakov, J. Janek, T. Brezesinski, *Chem. Mater.* **2024**, 36, 1497.
- [63] R. Rueß, D. Gomboso, M. Ulherr, E. Trevisanello, Y. Ma, A. Kondrakov, T. Brezesinski, J. Janek, *J. Electrochem. Soc.* **2023**, 170, 020533.
- [64] G. Mirabelli, C. McGeough, M. Schmidt, E. K. McCarthy, S. Monaghan, I. M. Povey, M. McCarthy, F. City, R. Nagle, G. Hughes, A. Cafolla, P. K. Hurley, R. Duffy, *J. Appl. Phys.* **2016**, 120, 125102.
- [65] H. Liu, N. Han, J. Zhao, *RSC Adv.* **2015**, 5, 17572.
- [66] W. Jaegermann, D. Schmeisser, *Surf. Sci.* **1986**, 165, 143.
- [67] L. Karger, K. Synnatschke, S. Settele, Y. J. Hofstetter, T. Nowack, J. Zaumseil, Y. Vaynzof, C. Backes, *Adv. Mater.* **2021**, 33, 2102883.
- [68] F. Walther, S. Randau, Y. Schneider, J. Sann, M. Rohnke, F. H. Richter, W. G. Zeier, J. Janek, *Chem. Mater.* **2020**, 32, 6123.
- [69] K. Homma, Y. Liu, M. Sumita, R. Tamura, N. Fushimi, J. Iwata, K. Tsuda, C. Kaneta, *J. Phys. Chem. C* **2020**, 124, 12865.
- [70] R. Zhang, F. Strauss, L. Jiang, L. Casalena, L. Li, J. Janek, A. Kondrakov, T. Brezesinski, *Chem. Commun.* **2023**, 59, 4600.
- [71] M. A. Bizeto, V. R. L. Constantino, *Mater. Res. Bull.* **2004**, 39, 1729.
- [72] T. Nakato, K. Kuroda, C. Kato, *Chem. Mater.* **1992**, 4, 128.
- [73] A. L. Shiguihara, M. A. Bizeto, V. R. L. Constantino, *Colloids Surf. B Biointerfaces* **2007**, 295, 123.
- [74] C. H. B. Silva, N. A. Galiote, F. Huguenin, É. Teixeira-Neto, V. R. L. Constantino, M. L. A. Temperini, *J. Mater. Chem.* **2012**, 22, 14052.